Identification of Johnson–Cook and Tresca's Parameters for Numerical Modeling of AISI-304 Machining Processes

Paolo Bosetti[1]
e-mail: paolo.bosetti@unitn.it

Carlos Maximiliano Giorgio Bort

Department of Industrial Engineering,
University of Trento,
Trento I-38123, Italy

Stefania Bruschi
Department of Industrial Engineering,
University of Padova,
Padova I-35131, Italy

This paper presents a procedure for the identification of Johnson Cook model parameters and Tresca's law friction factor for orthogonal cutting of AISI 304. The process is described by a thermomechanical numerical model. The parameters are identified by minimizing the error in the prediction of cutting force, chip thickness, and chip curvature. Two optimization algorithms where tested: a pure Nelder–Mead method (NMM), and a hybrid procedure, in which the starting simplex for NMM is calculated by means of a genetic algorithm. The results emphasize the importance of the initial guess chosen in the optimization to obtain a reliable set of parameters. By using the optimized parameters in the numerical model, the cutting force, the chip thickness, and the chip curvature can be evaluated with an acceptable accuracy. The identified rheological and tribological coefficients are validated for different orthogonal cutting conditions. [DOI: 10.1115/1.4025340]

1 Introduction

Machining processes are of fundamental importance in several fields of mechanical engineering. Different approaches tried to describe the mechanism underlaying the machining processes and to predict the process quality: empirical [1,2], theoretical [3], and numerical [4–6]. The latter approach is of greater interest for tool manufacturers and the mechanical industry, since it can provide the largest amount of information about the process.

It is well known that the reliability of numerical solutions depends not only on the model setup, but also on the thermomechanical, tribological, and rheological laws used to describe the behavior of the workpiece and its interaction with the cutting tool. This paper presents an optimization-based procedure for the simultaneous identification of the parameters used in Johnson– Cook's (JC) rheological model and in Tresca's tribological law. Traditionally, these parameters are identified through two different approaches:

(a) **direct**: dedicated experimental tests designed to provide a direct measure of rheological or tribological model parameters;
(b) **indirect**: identification by means of inverse analysis, which combines experimental and numerical techniques.

In both cases, rheological and tribological parameters are usually separately assessed.

Among the indirect methods, several authors developed hybrid empirical–numerical approaches based on the Split-Hopkinson pressure bar test [7,8] and on other types of tests [9]. These procedures involve static, quasi-static, and dynamic tests, and can be useful for processes characterized by strain rates up to $300\,s^{-1}$ and more [10,11], even at high temperature. As stated by Chandrasekaran et al. [12], due to the extreme strains and strain rates characterizing the cutting process, the pressure bar test cannot be used in the parameter identification of the material model for machining processes. By means of a numerical model of orthogonal cutting, the indirect method was also applied by Shrot and Bäker [13,14] to the identification of yield strength, hardening modulus, and hardening coefficient of the Johnson–Cook model. Bäker and Shrot [15] proposed a methodology to reduce the number of FEM simulations required to solve the identification problem, by defining knowledge-based descriptors that were approximately proportional to observable quantities. However, the definition of these descriptors appears to be problem-dependent and it generally requires a physical understanding of the problem, so it is not easily portable to different problems or processes.

Reliable JC parameters for AISI 304 are still lacking in the literature: indeed, it is possible to find references to significantly different sets of coefficients for a given material [16,17]. In a previous study [18], by comparing the poor accuracy of the results obtained by modeling the orthogonal tube cutting (OTC) process of AISI-304 with the different sets of JC parameters available in the literature, the Authors demonstrated the need for a procedure allowing robust parameters identification. The Authors developed an automated procedure for multi-objective optimization through a simplified version of the Nelder–Mead method applied to orthogonal cutting process simulated by using the FEA commercial software DEFORM. The results of that work showed that, although the cutting force can be correctly estimated, the predicted chip morphology does not match well with that of real chips. Moreover, it was observed that the target function was characterized by multiple minima, and therefore a more robust optimization algorithm had to be used.

This paper represents a step forward in this direction: here is investigated the feasibility of indirect, simultaneous identification of rheological and tribological parameters by using the NMM, the genetic algorithms method (GAM), and a hybrid method (HM) exploiting strengths of both NMM and GAM. The main characteristics of the first two approaches are outlined, and the need for applying an hybrid procedure is explained and commented. The HM has been applied successfully by several authors [19–21] to speed up the minimization of multimodal functions.

The reference machining test adopted hereafter for the parameters identification is the OTC test, carried out on relatively thin-walled tubes made of AISI-304 steel. The objective function is related to the model accuracy, which is assessed by calculating

[1]Corresponding author.

Contributed by the Manufacturing Engineering Division of ASME for publication in the JOURNAL OF MANUFACTURING SCIENCE AND ENGINEERING. Manuscript received March 28, 2013; final manuscript received August 19, 2013; published online September 23, 2013. Assoc. Editor: Donggang Yao.

Copyright © 2013 by ASME

Downloaded From: http://manufacturingscience.asmedigitalcollection.asme.org/ on 10/08/2013 Terms of Use: http://asme.org/terms

the relative error in the estimation of cutting force, chip thickness, and chip curvature. The input parameters of the optimization problem are the five coefficients of the JC model, plus the friction factor of the Tresca's law.

The paper is organized in four main sections, plus the final Conclusions section. Section 2 describes the experimental setup, i.e., the orthogonal cutting experiment that carried out for providing the values of observable quantities, on which the forthcoming identification is based. Section 3 illustrates the finite element model that has been developed for simulating a 2D approximation of the same orthogonal cutting experiment. Physical experiment results and numerical model are then used in conjunction for identifying the model parameters: the FE model is solved with different sets of parameters until the simulation results match the experimental results. Section 4 describes the optimization algorithms that have been adopted and implemented for adapting the FE model parameters by minimizing the difference between observable quantities obtained from model and from experiment. Finally, results of the proposed methodology are discussed in Sec. 5.

2 Experimental Setup

The OTC is a machining process, in which the cutting speed and feed rate vectors are perpendicular. In this study, such a configuration has been set up on a lathe, spinning the tube and feeding the tool along the tube axis (Fig. 1, left). The material chosen for the tube was the AISI-304 steel since it is a well-known material and there is a vast literature describing its properties. The external diameter of the tube was 50 mm, and its wall was 1 mm thick. The cutting tool was a TiN-coated HSS insert produced by Alesa AG (ISO code APFT 16 04 04 FR) whose rake angle was 18 ± 2 deg, and the inclination angle was zero. The cutting speed and feed rate were set to 26.77 m/min and 0.09 mm/rev, respectively, according to the data sheet given by the tool manufacturer.

The process performance was evaluated by measuring the cutting force, tool-chip contact length, chip thickness, and chip curvature. These outputs are indeed the most relevant for tool manufacturers and process planners since they are strictly related to the dynamics of the process, thus determining its quality. A Kistler multicomponent dynamometer mod. 9257B was placed below the toolholder to measure the cutting force.

Two different series of OTC tests were performed: a continuous tube turning for assessing the cutting forces, the tool–chip contact length, and the chip thickness; an interrupted, short-cut turning for producing a short chip suitable for measuring its curvature (Table 1).

In the first case, a continuous turning operation was performed starting with a new tool for a total cutting time of 2 min. In this way, it was obtained an evident wear on the tool rake face but before a getting an excessive modification of tool geometry. The cutting force was measured as an average value on the attainment of the steady state condition after the first contact of tool with the workpiece. Seven different chip segments were then observed on an environmental scanning electron microscope (ESEM) in order to measure the average chip thickness, and the same ESEM microscope was also used to measure the chip–tool contact length. On the tool rake face it was possible to observe a bright area, along which the backscattered electrons microanalysis allowed to further identify an area close to the cutting edge made by the same cutting tool material, followed by another area made by a layer of AISI-304 deposited during the cut (see Fig. 1, right). The former was assumed to be related to the constant contact zone, while the outer AISI-304 coated area was assumed to be the result of the intermittent contact between chip and tool due to chip vibrations. Consequently, only the width of former area was measured in order to determine the length of the contact zone.

In the second case, an interrupted cutting operation was performed in order to obtain a single chip of a length comparable to that obtained by the numerical model, as described in Sec. 3. The chip curvature was measured by means of an optical microscope in the chip zone immediately after the thickening due to the sudden tool stop, which is clearly visible in the bottom right image of Fig. 7.

The results of the measurements above described are reported in Table 1.

Table 1 Experimental measures on OTC tests

Measure	Value	Std. dev.
Cutting force (N)	182	8
Contact length (μm)	250	4
Chip thickness (mm)	105	8
Chip curvature (1/mm)	1.51	0.01

3 Numerical Model

The numerical model was implemented in the commercial FEA software DEFORM 2D v.10.2. This software allows the definition and solution of nonlinear thermomechanical problems, such as bulk deformations processes and cutting processes. In order to keep the solution time within feasible limits, it was possible to reduce the dimensionality of the OTC model by assuming a plane strain condition. This is justified by the reduced nominal feed rate (0.09 mm/rev) compared to the tube thickness (1 mm).

The rheology of the workpiece is described by the semi-empirical JC model, which is one the most complete models currently used in cutting simulation literature and is available within the DEFORM software. The JC model is formulated by the following equation [22]:

$$\sigma(T, \varepsilon, \dot{\varepsilon}) = (A + B\varepsilon^n)\left[1 + C ln\left(\frac{\dot{\varepsilon}}{\dot{\varepsilon}_0}\right)\right]\left[1 - \left(\frac{T - T_r}{T_m - T_r}\right)^m\right] \quad (1)$$

where A is the yield strength, B the hardening modulus, C the strain-rate sensitivity, n the hardening coefficient, m the thermal softening coefficient, ε the plastic strain, $\dot{\varepsilon}$ the strain rate, $\dot{\varepsilon}_0 = 1.0\,s^{-1}$ the effective plastic strain-rate of the quasi-static test

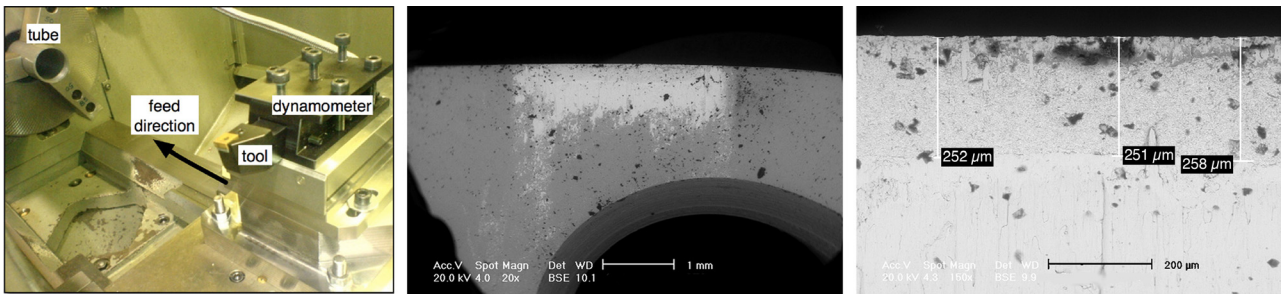


Fig. 1 The experimental setup used in the OTC test (left); SEM image of the tool rake with the worn area and the AISI-304 sticking zone (middle) and a particular of the tool rake face with measurements of the worn area (right)

Downloaded From: http://manufacturingscience.asmedigitalcollection.asme.org/ on 10/08/2013 Terms of Use: http://asme.org/terms

used to determine the yield and hardening parameters [7,16,17,23], T is the workpiece temperature, $T_m = 1454\,^{\circ}C$ the melting temperature, and $T_r = 20\,^{\circ}C$ the room temperature. The first five terms (i.e., A, B, C, n, and m) are the unknown parameters to be identified, while ε, $\dot{\varepsilon}$, and T are FE solution parameters.

Regarding the simulation of the chip/tool friction, several tribological models have been proposed in literature [24,25]. Given the high normal pressure produced by the chip on the tool rake face, the FE software has been set up adopting the Tresca's law for describing the tool–chip interaction. According to this model, the friction force saturates when the normal force on the tool rake face exceeds a fraction of the maximum admissible tangential stress

$$\tau = \eta\,\tau_Y = \eta A/\sqrt{3} \tag{2}$$

where τ is the tangential friction stress (a FE solution parameter), τ_Y the yield shear stress (assumed as $A/\sqrt{3}$ according to Von Mises), and η the friction factor (to be identified).

Figure 2 shows the mesh and the boundary conditions of the 2D FE model. The tool was modeled as a rigid material, and the workpiece as a plastic material, avoiding the elastic behavior since the residual stresses were not considered among the observables outputs. Mechanical and thermodynamical constraints were imposed on the workpiece. Null horizontal and vertical velocities were assumed on the bottom and the left edges. The latter was set at room temperature (20 °C), while the remaining sides exchanged heat with the environment and with the tool. The convection coefficient was set to $10\,W/m^2K$, while the heat transfer coefficient between the workpiece and the tool was set to $3000\,W/m^2\,K$ [18]. The process parameters were chosen accordingly to those used in the experimental test: depth of cut of 0.098 mm, cutting speed of 26.77 m/min, tool rake angle of 18 deg.

The time step was set to 5 μs and the cutting length was 5 mm to ensure the achievement of the steady state cutting condition. An adaptive mesh with quadrangular quadratic elements was used for tool workpiece, setting a maximum edge length of 6 μm) only in the area close to the cutting edge, thus reducing the simulation time.

4 Optimization Algorithms

The parameters identification problem is addressed as a multi-objective optimization problem, in which the input values are the set of JC parameters plus the friction factor of the Tresca's law. The target function $F_{target}(\mathbf{X})$ can be expressed as the weighted sum of the relative errors between the measured outputs and the calculated ones

$$F_{target}(\mathbf{X}) = \sum_{i=1}^{4} w_i \frac{|Y_{mi} - Y_{ci}|}{Y_{mi}} + p(\mathbf{X}) \tag{3}$$

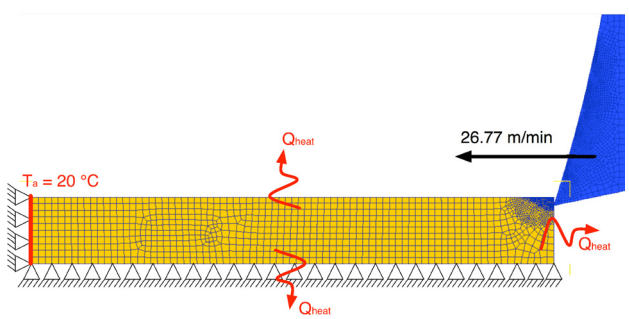


Fig. 2 The OTC test model implemented in DEFORM 2D

Table 2 Extremes of the domain of the JC and Tresca's coefficients for the first population

Parameter	A	B	C	N	m	η
Maximum	1000	1500	1	1	1	1
Minimum	10	50	0.01	0.01	0.01	0.01

Table 3 Starting simplex for the identification with randomly initialized NMM (r-NMM)

F_{target}	A	B	C	n	m	η
4.070	123.0	232.0	0.61	0.83	0.09	0.24
5.653	177.0	98.0	0.50	0.89	0.93	0.70
5.977	34.0	142.0	0.39	0.52	0.37	0.58
3.874	130.0	292.0	0.13	0.59	0.99	0.88
7.001	250.0	193.0	0.97	0.48	0.80	0.88
4.396	80.0	197.0	0.99	0.76	0.63	0.45
5.139	173.0	281.0	0.03	0.71	0.23	0.28

Table 4 Starting simplex for the identification with preconditioned NMM (p-NMM)

F_{target}	A	B	C	n	m	η	References
7.266	350.0	275.0	0.02	0.36	1.00	0.60	[16]
7.713	310.0	1000.0	0.07	0.65	1.00	0.50	[17]
8.063	1000.0	1500.0	0.01	0.36	1.00	0.90	R
8.000	239.0	522.0	0.10	0.65	1.00	0.70	[40]
7.547	128.9	84.9	0.02	0.97	0.46	0.40	D
6.306	982.0	513.0	0.23	0.20	0.93	0.97	R
5000.0	65.0	1067.0	0.26	0.46	0.41	0.74	R

Note: D = default values suggested by Deform and R = random value

Table 5 Starting simplex for the identification with hybrid GAM-preconditioned NMM (HM)

F_{target}	A	B	C	n	m	η
2.564	290.8	641.5	0.40	0.51	0.54	0.42
2.243	327.2	734.6	0.40	0.51	0.54	0.42
2.782	426.4	837.6	0.88	0.45	0.33	0.52
4.356	959.8	984.8	0.61	0.80	0.54	0.57
3.117	290.8	641.5	0.40	0.51	0.54	0.54
2.385	290.8	641.5	0.40	0.53	0.33	0.52
4.332	426.4	837.6	0.88	0.43	0.54	0.42

$$p(\mathbf{X}) = \sum_{j=1}^{6} \max(0, X_j - X_{max,j})^2 \tag{4}$$

where $\mathbf{Y}_m$ and $\mathbf{Y}_c$ are the vectors of four elements containing, respectively, the measured outputs and the calculated ones, $\mathbf{w}$ is the set of weights, and $\mathbf{X}$ and $\mathbf{X}_{max}$ are the vector of six elements representing the optimized parameters and their maximum values (see Tables 2–8), respectively. The term $p(\mathbf{X})$, finally, represents the constraints imposed on parameters in the form of penalties.

Since it is not possible to evaluate analytically the derivatives of the target function, two nonderivative algorithms were used for the optimization: the NMM, and a GAM. NMM is initialized in a small region of the target function; thus, it tends to reach a minimum in relatively few iterations, while its convergence is less robust and more prone to find local minima instead of the global ones. Conversely, the main advantage of evolutionary algorithms is related to their ability to find the global minimum even when a

Downloaded From: http://manufacturingscience.asmedigitalcollection.asme.org/ on 10/08/2013 Terms of Use: http://asme.org/terms

Table 6 Calculated performances of the identifications

Output	Measure	p-NMM	r-NMM	HM
Iterations	–	38	52	115
F_{target}	–	1.158	2.168	0.865
Cutting force (N)	182.0	195.8	182.1	171.0
(Error %)		(7.6)	(0.0)	(6.0)
Chip thickness (mm)	0.105	0.148	0.245	0.125
(Error %)		(40.8)	(133.4)	(19.1)
Chip curvature (1/mm)	1.51	1.331	0.491	1.415
(Error %)		(11.8)	(67.5)	(6.3)
Chip contact length (mm)	0.25	0.149	0.210	0.143
(Error %)		(40.4)	(15.8)	(42.9)

Table 7 Optimized rheological and tribological coefficients

Optimizer	A	B	C	n	m	η
r-NMM	118.2	255.3	0.61	0.59	0.47	0.47
p-NMM	530.4	670.7	0.22	0.16	0.51	0.82
HM	634.4	666.1	0.59	0.37	0.17	0.59

Table 8 Simulation of test cases in Ref. [41]

Cutting speed (m/min)	rake angle (deg)	feed (mm/rev)	Cutting force (N)
100	−8	0.1	1174 (1088)
200	−8	0.2	1841 (1888)

multiplicity of local minima is present. This is due to the stochasticity underlying the GAM, which allows them to explore different and distant regions of the domain, thus increasing the chances to find the global minimum. The characteristics of the NMM and GAM approaches will be discussed in Secs. 4.1 and 4.2.

4.1 Nelder–Mead Method. The Nelder–Mead method is a well-known method that can handle nonlinear and nondifferentiable functions [26]. It has been used in a wide spectrum of challenging problems: parameters identification [18,27], mechanical design [28], manufacturing processes optimization [29], microfabrications [30], nuclear energy production [31].

The NMM used in this work is based on a simplex on the six-dimensional response surface and implements the full set of simplex operations (i.e., reflection, expansion, contraction, and shrink).

The convergence criterium is based on the simplex norm ζ, defined as:

$$\zeta = \frac{1}{N}\sqrt{\sum_{i=1}^{N-1}\sum_{j=i+1}^{N}\left(F_{\text{target}}(X_i) - F_{\text{target}}(X_j)\right)^2} \tag{5}$$

where N is the dimension of the simplex, and X_i and X_j are the ith and jth vertices of the simplex. It is assumed that the optimization converged if when $\zeta < 10^{-6}$. Due to the nature of this method, when optimizing multimodal functions, the optimal point found by the algorithm depends on the simplex chosen at the initialization. This aspect is emphasized in this study where NMM will be initialized in three different ways: randomly, preconditioned accordingly to the solutions founds in literature, and from a near-optimal simplex calculated by a genetic algorithm.

4.2 Genetic Algorithm. Genetic algorithms are heuristic methods used to emulate the natural selection, evolving the optimal solution across a wide region of the target function domain. Each set of input variables, called *chromosome*, is typically encoded into a binary string. These strings are collected to form a *population*. The populations are then evolved during the iterations, keeping the chromosomes with a lower *fitness* (i.e., that have more chances to survive), and discarding or modifying those with the higher fitness. In optimization problems the fitness is the target function.

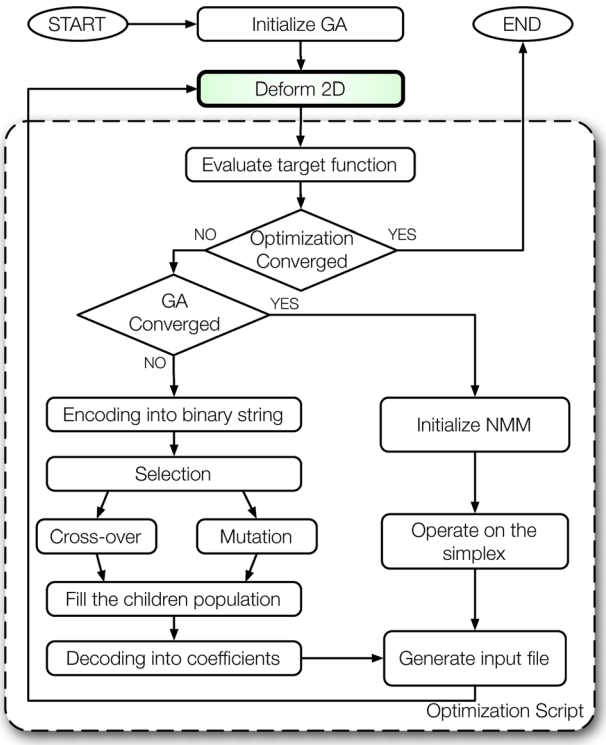


Fig. 3 Architecture of the identification procedure

Despite the usually high computational cost of numerical models, GAM has become extremely popular in recent years, thanks to the improved computers performances. Some authors used GAM for solving inverse analysis problems for parameter identification [32–35], other for building empirical models [36] or for performing a multi-objective optimization of cutting parameters [37].

In this study, the main task of the GAM is to find the more promising subdomain where to start the minimum search with a subsequent application of NMM. Consequently, the size of the GAM population has been chosen by considering that the number of chromosomes (i.e., different combinations of the six parameters to be identified) must be larger than a six-dimensional simplex (i.e., seven points in a 6D hyperspace). At the same time, given the high computational cost of calculating the fitness function for each chromosome, the actual number of chromosomes has been set to 20.

The architecture of the genetic algorithm implemented in this study is schematized in Fig. 3. The chromosomes in the first population are generated randomly within the limits reported in Table 2, which correspond to the wider domain still physically meaningful. The whole *parent* population is then evaluated, the individuals are sorted in ascending order according to their fitness, and encoded in to binary strings. This operation is performed by using a four-byte number for each element of the individual. The first bit is used to represent the sign (1 for negative numbers), 15 bits are used to represent the integer part, and 2 bytes are used for the decimal part. Four bytes for each one of the six parameters are then concatenated to form a 24 bytes binary, the chromosome. The first three individuals of the rank are moved into a new

Downloaded From: http://manufacturingscience.asmedigitalcollection.asme.org/ on 10/08/2013 Terms of Use: http://asme.org/terms

children population. A *selection* is then performed to complete the children. In this operation ten couples of chromosomes are randomly extracted from the parent and the best individual in each pair is moved to the children population. The remaining seven chromosomes that are needed to fill the population are created by means of two operations: *cross-over* and *mutation*. The former is performed with a probability $p_c = 0.8$ and generates two new individuals by exchanging part of the binary string of two randomly chosen chromosomes. In the mutation the value of a random bit in a noncrossed-over chromosome is inverted with a probability $p_m = 0.2$. As can be noted, the method has a strong stochastic component that guarantees variability across the population, therefore a large exploration area of the objective function. The values of p_c and p_m have high effect in the performance of GAM and must be carefully set. These were identified through a manual simplex method, and by using different test functions available in literature [38,39].

The GAM procedure ends if the difference between the fitness of the two best chromosomes is less than 0.1, and the best seven chromosomes are used as a starting point for the subsequent NMM application. Otherwise, the evolutionary process restarts from the selection.

4.3 Optimization Procedure. The identification procedure and the optimization algorithms were implemented in the Ruby programming language. A custom interface with DEFORM 2D has been developed, in order to enable the automated use of the FEA software by the optimization procedure, for the evaluation of the GAM fitness function and of the NMM target function.

Figure 3 summarizes the architecture of the identification procedure. Each optimization step generates a DEFORM 2D input file with the rheological and tribological parameters, which is used to create and solve the FEA model of the OTC. If the simulation does not converge, the target function is set to a high value, and the optimizer script proceeds to the next iteration. Conversely, if the convergence is reached, the optimizer script analyzes the model calculating the average cutting force achieved at the steady state conditions, the tool–chip contact length, the chip thickness, and its curvature.

The chip geometry and the tool–chip contact length are calculated by analyzing the model configuration (i.e., the nodal positions) at the final simulation step. In Fig. 4, the tool is fed from right to left. The green cross marks represent the chip nodes, which are denser around the cutting edge due to remeshing criterium set in the FE software. The black asterisks are the nodes at the tool–chip interface, and are used to calculate the tool–chip contact length, evaluated as the sum of the distances between nearest neighbors nodes.

To calculate the chip thickness and its curvature, it is necessary to localize the nodes on its internal and external edges. This operation has to be robust since it must handle both odd-shaped and highly curved chips as well. Therefore, first of all the nodes lying below the upper unmachined workpiece surface are discarded (notice the missing nodes in the bottom and upper part of the chip, areas A and B, respectively, in Fig. 4). Then, a rough estimate of chip thickness is calculated as the minimum distance between each node on the internal chip surface and each node on the external one. Note that this estimate can be affected by local noise (also related to the mesh size), so a second step is performed in order to have a more robust estimate. In this second step, a subset of the surface nodes is selected, so that their distance from the cutting edge is less than 4 times the previously estimated chip thickness. The two sets of surface nodes (internal and external) are then interpolated with two circular arcs, whose difference in radius gives the chip thickness. The inverse of the average radius between the two circles is assumed as the chip curvature.

Once the four outputs have been calculated, the target function is evaluated by Eq. (3), using the set of weights $w_1 = 3$ (cutting force component) and $w_{2\ldots4} = 1$. A higher weight is associated to the cutting force since it represents the most important observable that influences the process dynamics, as a preliminary sensitivity analysis performed on the FEM model pointed out. If the convergence criterium for the GAM is satisfied, an optimal simplex is built—taking the best seven chromosomes in the last population—and the identification proceeds with the NMM, until the simplex norm as defined in Eq. (5) becomes less than 10^{-6}.

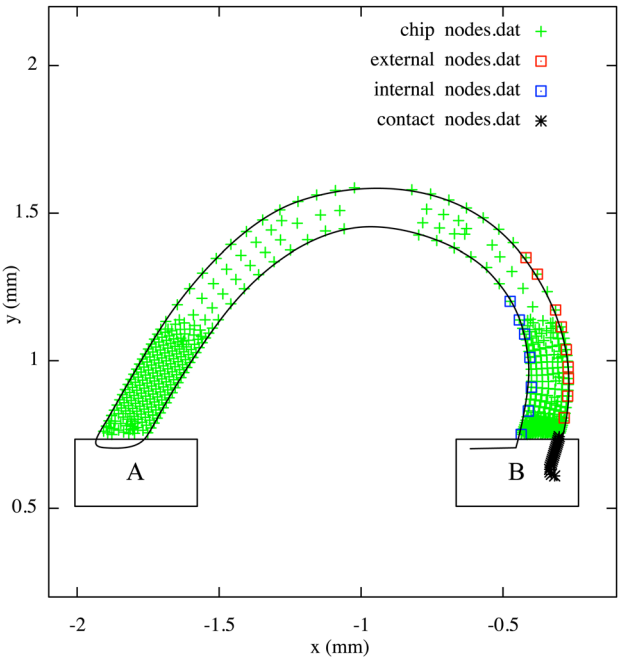


Fig. 4 Analysis performed on the chip nodes at the end of the simulation. The tool moves from right to left

5 Results

According to the considerations above expressed, the identification of the JC and Tresca's parameters has been performed by following three different approaches for initializing the simplex. The first is based on a completely random simplex initialization (r-NMM, obtained through a uniform sampling of coefficients within the domain reported in Table 2). The results of this simplex generation are reported in Table 3.

In the second approach, referred to as p-NMM, the simplex was partially initialized with the default values suggested by DEFORM, three sets of coefficients available in the literature [17,16,40], and the remaining three vertices were generated randomly. The results are reported in Table 4. Note that for the last combination in Table 4, the FE solution was not converging, so an arbitrarily high value $F_{\text{target}} = 5000.0$ was manually set in order to penalize that configuration.

In the last case, the identification was performed through the above described HM approach, in which the NMM was initialized with a suboptimal simplex calculated by the GAM. In turn, the GAM converged to the threshold as described in Sec. 4.2 after five generations of 20 chromosomes. The results are reported in Table 5. By comparing the values of the target function in the three initial guesses, it can be noted that the HM is the method that gives the best starting simplex.

The results obtained by the three identification approaches are summarized in Table 6. The best minima is calculated by the HM after 115 simulations (including 5 GAM iterations of 20 simulations each, plus 15 NMM iterations), by virtue of the suboptimal starting simplex configuration that was previously calculated through the GAM. The good performance of the HM is further emphasized by the relatively quick evolution of the best simplex vertex during the optimization, as shown in Fig. 5.

Downloaded From: http://manufacturingscience.asmedigitalcollection.asme.org/ on 10/08/2013 Terms of Use: http://asme.org/terms

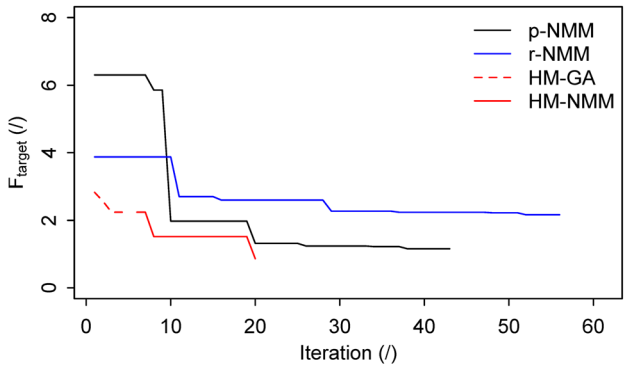


Fig. 5 Convergence plot

Moreover—even though a random initialization could lead to a simplex with smaller value of F_{target} than that obtainable by the preconditioned initialization—the physical relevance of the rheological and tribological coefficients and the NMM convergence are not guaranteed. Furthermore, the r-NMM requires 52 iterations to converge, while the p-NMM converges after 38 iterations.

The cutting force is the most important observable of the cutting process. It ramps up to the steady state condition after a short transient lasting 0.001 s, as shown in Fig. 6. All the identifications can correctly predict the cutting force, as result of the higher weight that has been assigned to it in the target function, according to Eq. (3). With respect to the best set of coefficients calculated by the HM, it is possible to conclude that the results on the chip thickness and chip curvature are also satisfactory, as confirmed by Fig. 7 reporting the comparison between real and calculated chip shapes.

The tool–chip contact length is the only process output that is not correctly predicted by the FEA simulation, even when considering the set of process parameters with the lowest value of F_{target}. This fact could not only depend on the inaccuracies associated to the rheological and tribological coefficients, but also on the experimental criteria chosen to estimate the tool–chip contact area. In fact, a relatively high uncertainty is associated to this measurement, especially due to the often subjective analysis and interpretation of the wear patterns and features characterizing the tool rake face.

The sets of rheological and tribological coefficients identified by the three methods are summarized in Table 7. One can observe that the sets of coefficients calculated by the HM and by the p-NMM differ slightly, especially as regards η. Moreover, the set of coefficients identified by the r-NMM identification is physically meaningless, since the values of yield strength, A, and hardening modulus, B, are too small to be associated with the stainless steel AISI-304 modeled in the simulations.

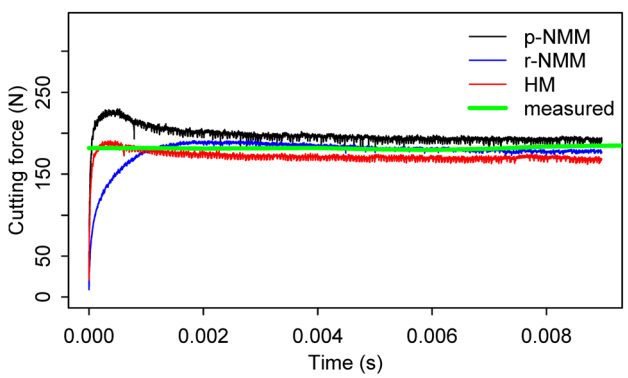


Fig. 6 Measured and calculated cutting force

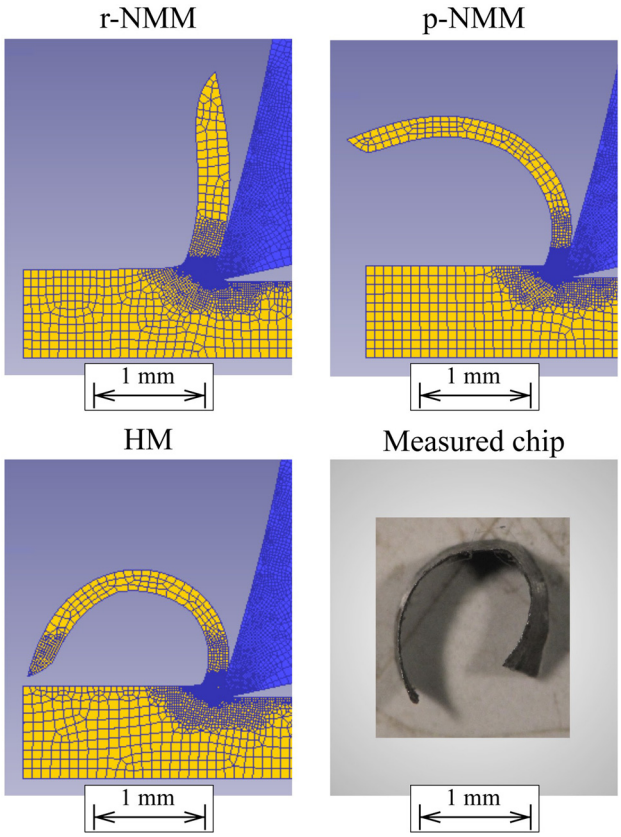


Fig. 7 Calculated and measured chips

At this point, an important observation has to be made. The inverse analysis here presented aims at identifying six parameters through four observables obtained from a single experimental condition. Strictly speaking, the optimization procedure is thus ill-conditioned. As such, the uniqueness of the solution cannot be granted, unless more than one experimental set of parameters is considered. Nevertheless, by perturbing the six parameters within the NM scheme about the solution obtained by HM it was possible to observe that the optimized set is a local stationary point (i.e., variation of parameters along any arbitrary direction on the response surface produces a worse fit). Additionally, the same set of optimal parameters obtained from HM has been used to simulate the different operating conditions for orthogonal cutting reported in D'Urso and Attanasio [41], obtaining very similar values for cutting force from model as from real experiments (see Table 8, real values in parentheses).

Such a dichotomy can be explained by considering that the four observables are not local evaluations of Eqs. (1) and (2), but rather macroscopic observations of a collective effect produced by the stress–strain field, whose intrinsic multiplicity helps reducing the ill-conditioning. Additionally, the model under identification is actually based on an empirical model. Indeed, there is no guarantee that the JC model will provide the accurate description of the material behavior over the whole domain. So, even if the identification had been performed covering more than one experimental condition, there would be no guarantee for the identified set of parameters to provide a better fit around a single configuration.

In other words, the procedure here presented (specifically, the HM-based variant) represents the identification of a complex numerical–empirical model, embodied by the FE software system. Identification of such a system is much like training of a neural network: if one is not interested on the physical significance of the weights of the neurons, the network is reliable until it is applied on a domain, which has to be close enough to the training domain. Likewise, the parameters identified in Sec. 4 can be effectively

Downloaded From: http://manufacturingscience.asmedigitalcollection.asme.org/ on 10/08/2013 Terms of Use: http://asme.org/terms

used to simulate process condition close enough to the one used for identification, as demonstrated by Table 8. Trying to expand the domain, over which the results obtained by the model remain accurate, by increasing the number of experimental test cases, could as well bring to unexpected or less accurate results, since there is no guarantee that the empirical black-box represented by the FE software based on the JC and Tresca models can actually fit the reality over a larger domain. Within these assumptions, the proposed methodology is robust according to the initial aims, in the sense that it is less sensitive to local minima and to the initial choice of parameters for the inverse analysis, thus providing more reliable and repeatable results.

6 Conclusions

This paper presents a numerical model of the orthogonal tube cutting test, and a procedure for the identification by simultaneous inverse analysis of rheological and tribological model parameters. The inverse analysis was based on an experimental setup for orthogonal tube cutting, allowing the measurement of the cutting force (on-line), the chip thickness, the chip curvature, and the tool–chip contact length (off-line). The numerical model was developed in DEFORM 2D, and the identification was treated as an optimization problem, addressed by means of three custom implementations of nonderivative minimization algorithms. The coefficients of the Johnson Cook constitutive model and the friction factor of the Tresca's law were identified simultaneously. The best set of model coefficients was calculated by a hybrid Genetic algorithms-Nelder Mead method, while the worst set of coefficients was calculated by the randomly initializing NMM. The cutting force, chip thickness, and chip curvature resulting from the FEA simulation with the optimal set of coefficients identified by HM resulted to be acceptably close to those measured on the experimental setup.

The results emphasize the importance of a good starting guess for the NMM when it is used for the parameters identification. The proposed hybrid formulation can represent an effective and viable solution for inverse analysis of cutting processes, especially when there is only limited knowledge about the material and friction models. Finally, although a single set of experimental conditions has been used for model identification, the identified FE model has been used for simulating similar cutting experiments available in literature, and the cutting force calculated by the model proved to be reasonably close to the actual force values reported in the same literature reference.

References

[1] Benardos, P., and Vosniakos, G., 2002, "Prediction of Surface Roughness in CNC Face Milling Using Neural Networks and Taguchi's Design of Experiments," Rob. Comput. Integr. Manuf., **18**, pp. 343–354.

[2] Sivasakthivel, P., Murugan, V. V., and Sudhakaran, R., 2010, "Prediction of Tool Wear From Machining Parameters by Response Surface Methodology in End Milling," Int. J. Eng. Sci. Technol., **6**, pp. 1780–1789.

[3] Fang, N., Jawahir, I. S., and Oxley, P. L. B., 2001, "A Universal Slip-Line Model With Non-Unique Solutions for Machining With Curled Chip Formation and a Restricted Contact Tool," Int. J. Mech. Sci., **43**, pp. 557–580.

[4] Movahhedy, M., Gadala, M., and Altintas, Y., 2000, "Simulation of the Orthogonal Metal Cutting Process Using an Arbitrary Lagrangian Eulerian Finite-Element Method," J. Mater. Process. Technol., **103**, pp. 267–275.

[5] Umbrello, D., M'Saoubi, R., and Outeiro, J., 2005, "Three-Dimensional Thermo–Elastic–Plastic Coupled FEM Simulations for Metal Oblique Cutting Processes," J. Mater. Process. Technol., **168**, pp. 42–48.

[6] Shi, J., and Liu, C., 2004, "The Influence of Material Models on Finite Element Simulation of Machining," ASME J. Manuf. Sci. Eng., **126**(4), pp. 849–857.

[7] Dorogoy, A., and Rittel, D., 2009, "Determination of the Johnson-Cook Material Parameters Using the SCS Specimen," Exp. Mech., **49**, pp. 881–885.

[8] Vural, M., Rittel, D., and Ravichandran, G., 2003, "Large Strain Mechanical Behavior of 1018 Cold-Rolled Steel Over a Wide Range of Strain Rates," Metall. Mater. Trans., **34A**, pp. 2873–2885.

[9] Allen, D., Rule, W., and Jones, S., 1997, "Optimizing Material Strength Constants Numerically Extracted From Taylor Impact Data," Exp. Mech., **37**, pp. 333–338.

[10] Hokka, M., Kokkonen, J., Seidt, J., Matrka, T., Gilat, A., and Kuokkala, V.-T., 2012, "High Strain Rate Torsion Properties of Ultrafine-Grained Aluminum," Exp. Mech., **52**(2), pp. 195–203.

[11] Hokka, M., Leemet, T., Shrot, A., Baeker, M., and Kuokkala, V.-T., 2012, "Characterization and Numerical Modeling of High Strain Rate Mechanical Behavior of Ti-15-3 Alloy for Machining Simulations," Mater. Sci. Eng. A, **550**, pp. 350–357.

[12] Chandrasekaran, H., M'Saoubi, R., and Chazal, H., 2005, "Modelling of Material Flow Stress in Chip Formation Process From Orthogonal Milling and Split Hopkinson Bar Tests," Mach. Sci. Technol., **9**, pp. 131–145.

[13] Shrot, A., and Bäker, M., 2011, "How to Identify Johnson-Cook Parameters From Machinning Simulations," Proceedings of the 14th International ESAFORM Conference on Material Forming, AIP Conference Proceedings, pp. 29–34.

[14] Shrot, A., and Bäker, M., 2012, "Determination of Johnson-Cook Parameters From Machining Simulations," Comput. Mater. Sci., **52**(1), pp. 298–304.

[15] Bäker, M., and Shrot, A., 2013, "Inverse Parameter Identification With Finite Element Simulations Using Knowledge-Based Descriptors," Comput. Mater. Sci., **69**(0), pp. 128–136.

[16] Ocaña, J., Morales, M., Molpeceres, C., García, O., Porro, J., and García-Ballesteros, J., 2008, "Numerical Modelling and Experimental Characterization of Short Pulse Laser Microforming of Thin Metal Sheets," Proc. of the 4M2008 Conference Multi-Mater. Micro Manuf., Cardiff, UK, September 9–11, pp. 131–145.

[17] Mori, L., Lee, S., Xue, Z., Vaziri, A., Queheillalt, D., Dharmasena, K., Wadley, H., Hutchinson, J., and Espinosa, H. D., 2007, "Deformation and Fracture Model on Sandwich Structures Subjected to Underwater Impulsive Loads," J. Mech. Mater. Struct., **10**, pp. 1981–2006.

[18] Bort, C. G., Bruschi, S., and Bosetti, P., 2011, "Johnson Cook Parameter Identification for AISI-304 Machining Through Nelder-Mead Method," Proceedings of the XI International Conference on Computational Plasticity Fundamentals and Applications, pp. 1–12.

[19] Chelouah, R., and Siarry, P., 2003, "Genetic and Nelder-Mead Algorithms Hybridized for a More Accurate Global Optimization of Continuous Multiminima Functions," Eur. J. Oper. Res., **148**, pp. 335–348.

[20] Mendez, A., and Coello, C., 2009, "A New Proposal to Hybridize the Nelder-Mead Method to a Differential Evolution Algorithm for Constrained Optimization," 2009 IEEE Congress on Evolutionary Computation, CEC 2009, art. no. 4983268, pp. 2598–2605.

[21] Pang, L., and Kishawy, H., 2012, "Modified Primary Shear Zone Analysis for Identification of Material Mechanical Behavior During Machining Process Using Genetic Algorithm," ASME J. Manuf. Sci. Eng., **134**(4), p. 041003.

[22] Johnson, G., and Cook, W., 1983, "A Constitutive Model and Data for Metals Subjected to Large Strains, High Strain Rate, and Temperatures," Proceedings of the 7th International Symposium on Ballistics, The Hague, The Netherlands, April 19–21, pp. 1–7.

[23] Yan, H., Hua, J., and Shivpuri, R., 2007, "Flow Stress of AISI H13 Die Steel in Hard Machining," Mater. Des., **28**, pp. 272–277.

[24] Usui, E., and Shirakashi, T., 1982, "Mechanics of Machining—From Descriptive to Predictive Theory, on the Art of Cutting Metals—75 Years Later," Vol. PED 7, ASME Publications.

[25] Childs, T., 1998, "Material Property Needs in Modeling Metal Machining," Proceedings of the CIRP International Workshop on Modeling of Machining Operations, pp. 193–202.

[26] Mathews, J., and Fink, K., 2004, *Numerical Methods Using Matlab*, 4th ed., Prentice-Hall, Upper Saddle River, NJ.

[27] Wang, L., Xu, Y., and Li, L., 2011, "Parameter Identification of Chaotic Systems by Hybrid Nelder-Mead Simplex Search and Differential Evolution Algorithm," Expert Syst. Appl., **38**, pp. 3238–3245.

[28] Zahara, E., and Kao, Y., 2009, "Hybrid Nelder-Mead Simplex Search and Particle Swarm Optimization for Constrained Engineering Design Problems," Expert Syst. Appl., **38**, pp. 3880–3886.

[29] Sonmez, F., and Akbulut, M., 2007, "Process Optimization of Tape Placement for Thermoplastic Composites," Composites, **38**, pp. 2013–2023.

[30] Cernivec, G., Krc, J., Smole, F., and Topic, M., 2006, "Band-Gap Engineering in CIGS Solar Cells Using Nelder-Mead Simplex Optimization Algorithm," Thin Solid Films, **511–512**, pp. 60–65.

[31] Sacco, W., Filho, H., Henderson, N., and de Oliveira, C., 2007, "A Metropolis Algorithm Combined With Nelder-Mead Simplex Applied To Nuclear Reactor Core Design," Nucl. Energy, **35**(5), pp. 861–867.

[32] Franulović, M., Basan, R., and Prebil, I., 2009, "Genetic Algorithm in Material Model Parameters' Identification for Low-Cycle Fatigue," Comput. Mater. Sci., **45**, pp. 505–510.

[33] Aguir, H., BelHadjSalah, H., and Hambli, R., 2011, "Parameter Identification of an Elasto-Plastic Behaviour Using Artificial Neural Networks-Genetic Algorithm Method," Mater. Des., **32**, pp. 48–53.

[34] Nyarko, E., and Scitovski, R., 2004, "Solving the Parameter Identification Problem of Mathematical Models Using Genetic Algorithms," Appl. Math. Comput., **153**, pp. 651–658.

[35] Kang, Y., Lin, X., and Qin, Q., 2004, "Inverse/Genetic Method and Its Application in Identification of Mechanical Parameters of Interface in Composite," Compos. Struct., **66**, pp. 449–458.

[36] Zadshakoyan, M., and Pourmostaghimi, V., 2012, "Genetic Equation for the Prediction of Tool-Chip Contact Length in Orthogonal Cutting," Eng. Appl. Artif. Intell., **26**, pp. 1725–1730.

Downloaded From: http://manufacturingscience.asmedigitalcollection.asme.org/ on 10/08/2013 Terms of Use: http://asme.org/terms

[37] Quiza Sardiñas, R., Rivas Santana, M., and Brindis, E. A., 2006, "Genetic Algorithm-Based Multi-Objective Optimization of Cutting Parameters in Turning Processes," Eng. Appl. Artif. Intell., **19**(2), pp. 127–133.
[38] Luksan, L., and Vlcek, J., 2003, *Test Problems for Unconstrained Optimization*, Institute of Computer Science, Academy of Sciences of the Czech Republic, Prague, Czech Republic.
[39] Moré, J., Garbow, B., and Hillstrom, K. E., 1981, "Testing Unconstrained Optimization Software," ACM Trans. Math. Softw., **7**, pp. 17–41.
[40] Aquaro, D., 2006, "Erosion Rate of Stainless Steel Due to the Impact of Solid Particles," Proceedings of AITC-AIT 2006 International Conference on Tribology.
[41] D'Urso, G., and Attanasio, A., 2011, "Analytical and Numerical Modeling of Strain Hardening in AISI 304 Steel Cutting," Adv. Mater. Res., **223**, pp. 381–390.

Downloaded From: http://manufacturingscience.asmedigitalcollection.asme.org/ on 10/08/2013 Terms of Use: http://asme.org/terms